Array Optimization for Maximum Beam Collection Efficiency to an Arbitrary Receiving Plane in the Near Field

SEISHIRO KOJIMA (Graduate Student Member, IEEE), **TOMOHIKO MITANI** (Member, IEEE),
AND NAOKI SHINOHARA (Senior Member, IEEE)

Research Institute for Sustainable Humanosphere, Kyoto University, Kyoto 611-0011, Japan
CORRESPONDING AUTHOR: S. KOJIMA (e-mail: kojima.seishiro.33a@st.kyoto-u.ac.jp)

ABSTRACT In this article, an array optimization method for maximizing beam collection efficiency (BCE) to an arbitrary receiving plane in the near field is proposed. The proposed method considers each element pattern in an array; thus, optimization with mutual coupling is possible by using active element patterns. Besides, the proposed method can consider the polarization direction of a receiving antenna since the optimization problem is calculated in vector form. The problem of maximization of BCE boils down to the generalized eigenvalue problem, and the best solution can be obtained mathematically. The results obtained via numerical analysis in various calculation models indicate the validity of the proposed method. Optimization is then performed using the active element patterns obtained from electromagnetic simulation. Based on the comparison of the results without considering mutual coupling in the optimization, it is confirmed that the proposed method yields better results, such as lower reflection and antenna losses and higher BCE and transmission efficiency, by using active element patterns.

INDEX TERMS Active element pattern, array antenna, beam collection efficiency, mutual coupling, microwave power transmission, near field.

I. INTRODUCTION

MICROWAVE power transmission (MPT) can deliver energy to distant electronic devices, including high-altitude airship, wireless sensors, and unmanned aerial vehicles [1], [2], [3]. In MPT systems, efficient transmission of microwave to the receiving targets is one of the important issues. As a key factor to discuss the issue, beam collection efficiency (BCE) is defined as the ratio of the incident power on the receiving plane (Rx plane) to the total radiated power.

The optimization of array antenna parameters, such as array weights and element positions, is required to obtain the maximum BCE. Thus far, numerous researchers have investigated optimization for maximizing BCE, and various methods assuming the transmission in the far field have been proposed. Some optimization methods that can be employed to mathematically obtain the optimized array

weight have been introduced, such as exploitation of the discrete prolate spheroidal sequences [4] and solving of the generalized eigenvalue problem [5]. Moreover, the problem of optimization can be solved by using some methods for numerical optimization, such as linear programming problem [6], convex programming and compressive sensing [7], k-means algorithm for clustered planar arrays [8], chaotic particle swarm optimization with multiple constraints [9], and optimization using Bezier curves [10]. By employing multi-objective optimization, the method for simultaneously optimizing BCE and the shape of the flat-top radiation pattern has been proposed [11]. As previously described, the optimization methods in the far field are matured. Contrarily, studies on the optimization method in the near field are scarce, even though transmission in the near field is required for obtaining high BCE. This is probably because the near field radiation pattern on a Rx plane can be

approximated to the far field pattern when giving a quadratic phase taper to an array weight obtained through optimization in the far field [12]. The results obtained through far field optimization are available in the near field by giving a quadratic phase taper to focus on the Rx plane. However, the method is limited when the Rx plane is parallel with the transmitting antenna (Tx antenna) and is near the normal axis at the center of the Tx antenna, since the theory is based on the paraxial approximation. Thus, when the Rx plane is located away from the Tx antenna and the Rx plane is rotated, the theory cannot be applied. The BCE optimization for an arbitrary Rx plane in the near field needs to be calculated in vector form, although most optimizations in the far field are calculated in scalar form.

The method that uses S parameters between the transmitting and receiving antenna ports was introduced in [13] as an optimization method in the near field. This method can be employed even when obstacles are in the propagation region. Conversely, in large array antennas, all S parameters need to be calculated, and such calculation is of high cost. Based on the vector calculation, the BCE optimization method has been proposed, which boils down to the generalized eigenvalue problem. Thus, the optimized solution is obtained mathematically [14]. Despite the applicability of the optimization method to an arbitrary Rx plane, a detailed analysis has not been conducted. Also, in the previous study, the influence of each element pattern was not considered. In the near field, consideration of each element pattern is necessary. This is because the angles from each element to an observation point are not identical, and the influence of mutual coupling is reflected in each element pattern.

In this article, an optimization method for maximizing BCE to an arbitrary Rx plane in the near field is proposed. It should be noted that in this article, the near field indicates the Fresnel region (radiative near field). Although most optimization methods do not consider mutual coupling, the proposed method enables optimization including mutual coupling by using active element patterns, which are obtained from an electromagnetic simulation, since the influence of each element pattern is reflected in the proposed method. The remainder of this article is organized as follows. Section II formulates the optimization problem mathematically, and Section III presents the numerical results. Section IV describes the optimization method including mutual coupling and the simulation results. Section V concludes this article.

II. PROBLEM FORMULATION

This work focuses on the transmission from a two-dimensional array to an arbitrary Rx plane in the near field. In Fig. 1, the calculation model is presented. An observation point on an arbitrary plane is obtained using the following step. Assuming that the Rx plane is on the xy plane and the center is at the origin, an observation point on the receiving plane is given by $q = (x, y, 0)$. The rotation matrices denoting the rotation around the x, y, and z axes in the
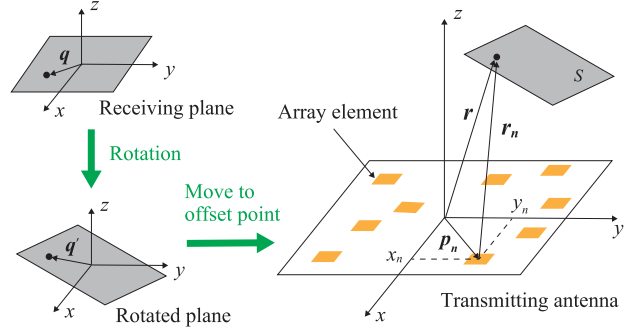

FIGURE 1. Calculation model in the near field.

three-dimensional space are defined respectively as follows:

$$R_x(\theta_x) = \begin{bmatrix} 1 & 0 & 0 \\ 0 & \cos\theta_x & -\sin\theta_x \\ 0 & \sin\theta_x & \cos\theta_x \end{bmatrix}, \quad (1)$$

$$R_y(\theta_y) = \begin{bmatrix} \cos\theta_y & 0 & \sin\theta_y \\ 0 & 1 & 0 \\ -\sin\theta_y & 0 & \cos\theta_y \end{bmatrix}, \quad (2)$$

$$R_z(\theta_z) = \begin{bmatrix} \cos\theta_z & -\sin\theta_z & 0 \\ \sin\theta_z & \cos\theta_z & 0 \\ 0 & 0 & 1 \end{bmatrix}, \quad (3)$$

where θ_x, θ_y, and θ_z denote the rotation angles for each axis, respectively, and the rotation direction is equal to the right-hand screw. Using the rotation matrices, the point on the rotated plane is expressed by the following equation:

$$q' = R_z(\theta_z)R_y(\theta_y)R_x(\theta_x)q. \quad (4)$$

Second, moving the receiving plane by the offset vector $q_{off} = [x_{off}, y_{off}, z_{off}]^T$, where z_{off} denotes the transmission distance, the position vector of the point on the receiving plane is given by $r = q' + q_{off}$. For a two-dimensional array antenna composed of N elements, with the n-th element position vector set to $p_n = (x_n, y_n, 0)$, the vector from the n-th element to the observation point is expressed by $r_n = r - p_n$. The radiated patterns of E-field and H-field are denoted by:

$$E(r) = \sum_{n=1}^{N} e_n(r_n) w_n \frac{e^{-jk_0 r_n}}{r_n}, \quad (5)$$

$$H(r) = \sum_{n=1}^{N} h_n(r_n) w_n \frac{e^{-jk_0 r_n}}{r_n}, \quad (6)$$

where $r_n = |r_n|$, w_n denotes the weight of the n-th element, and k_0 denotes the free-space wavenumber. $e_n(r_n) = [e_{nx}(r_n), e_{ny}(r_n), e_{nz}(r_n)]^T$ and $h_n(r_n) = [h_{nx}(r_n), h_{ny}(r_n), h_{nz}(r_n)]^T$ are the E-field and H-field radiation patterns of the n-th element, respectively. Note that e_{nx} denotes the x component of the n-th element's E-field. We assume that the calculation deals with the near field from the viewpoint of the array antenna, whereas the region is in the far field from the viewpoint of each element. Thus, the

E-field and H-field of each element are related, as expressed below:

$$h_n(r_n) = \frac{1}{Z_0}\hat{r}_n \times e_n(r_n), \tag{7}$$

where $\hat{r}_n$ denotes the unit vector of r_n. The x component of $E(r)$ and $H(r)$ are rewritten into the following vector forms:

$$E_x(r) = w^H v_{e_x}(r), \tag{8}$$

$$H_x(r) = w^H v_{h_x}(r), \tag{9}$$

$$v_{e_x} = \left[\frac{e_{1x}(r_1)}{r_1}e^{-jk_0 r_1}, \ldots, \frac{e_{Nx}(r_N)}{r_N}e^{-jk_0 r_N}\right]^T, \tag{10}$$

$$v_{h_x} = \left[\frac{h_{1x}(r_1)}{r_1}e^{-jk_0 r_1}, \ldots, \frac{h_{Nx}(r_N)}{r_N}e^{-jk_0 r_N}\right]^T, \tag{11}$$

where $w = [w_1, \ldots, w_N]^H$. The y and z components of $E(r)$ and $H(r)$ are also rewritten into the vector form by changing the subscript of x in (8)–(11) to y and z, respectively. In the near field, the received power P_r is calculated via the integration of the Poynting vector within the Rx plane. Using the vector forms previously mentioned, the z component of the Poynting vector $S = \frac{1}{2}(E \times H^*)$, $*$ denoting complex conjugate, is expressed by:

$$
\begin{aligned}
S_z &= \frac{1}{2}\left(E_x H_y^* - E_y H_x^*\right) \\
&= \frac{1}{2}\left\{w^H v_{e_x}(w^H v_{h_y})^* - w^H v_{e_y}(w^H v_{h_x})^*\right\} \\
&= \frac{1}{2}w^H\left(v_{e_x}v_{h_y}^H - v_{e_y}v_{h_x}^H\right)w = \frac{1}{2}w^H A_z w. \tag{12}
\end{aligned}
$$

Note that $(a^H b)^* = b^H a$ is employed and $A_z = v_{e_x}v_{h_y}^H - v_{e_y}v_{h_x}^H$. The x and y components of the Poynting vector are also written similar to (12) and are expressed by the following equations:

$$S_x = \frac{1}{2}w^H\left(v_{e_y}v_{h_z}{}^H - v_{e_z}v_{h_y}^H\right)w = \frac{1}{2}w^H A_x w, \tag{13}$$

$$S_y = \frac{1}{2}w^H\left(v_{e_z}v_{h_x}{}^H - v_{e_x}v_{h_z}{}^H\right)w = \frac{1}{2}w^H A_y w. \tag{14}$$

The received power P_r is obtained by the surface integral of the Poynting vector:

$$P_r = \int_s \Re(S) \cdot ds, \tag{15}$$

where s denotes the area of the Rx plane, $ds = ds\hat{n}$, and $\hat{n} = [\hat{n}_x, \hat{n}_y, \hat{n}_z]^T$ denotes the unit normal vector on the Rx plane outside the propagation direction. Since the unit normal vector is $\hat{z} = [0, 0, 1]^T$ before the Rx plane rotation, $\hat{n}$ is given as follows:

$$\hat{n} = R_z(\theta_z)R_y(\theta_y)R_x(\theta_x)\hat{z}. \tag{16}$$

From (12)–(16), the receiving power (15) is rewritten as follows:

$$
\begin{aligned}
P_r &= \int_s \Re(S_x\hat{n}_x + S_y\hat{n}_y + S_z\hat{n}_z)ds \\
&= \int_s \Re\left\{w^H\left(\frac{\hat{n}_x A_x + \hat{n}_y A_y + \hat{n}_z A_z}{2}\right)w\right\}ds
\end{aligned}
$$

$$
\begin{aligned}
&= \Re\left[w^H\left\{\int_s\left(\frac{\hat{n}_x A_x + \hat{n}_y A_y + \hat{n}_z A_z}{2}\right)ds\right\}w\right] \\
&= \Re\left(w^H A w\right), \tag{17}
\end{aligned}
$$

$$A = \frac{1}{2}\int_s(\hat{n}_x A_x + \hat{n}_y A_y + \hat{n}_z A_z)ds. \tag{18}$$

The matrix A is not a Hermitian matrix, and it needs to take the real part of $w^H A w$, making it difficult to calculate in this form. For any square matrix U, the matrix V obtained by $V = (U + U^H)/2$ becomes a Hermitian matrix. Moreover, assuming an arbitrary row vector x, the real part of $x^H U x$ is rewritten as follows [14]:

$$\Re\left(x^H U x\right) = x^H V x \tag{19}$$

Using the above theorem, (17) is eventually rewritten by

$$
\begin{aligned}
P_r &= \Re\left(w^H A w\right) = w^H\left(\frac{A^H + A}{2}\right)w \\
&= w^H B w, \tag{20}
\end{aligned}
$$

where $B = (A^H + A)/2$. The total radiated power P_t is obtained by the surface integral of Poynting vector in all solid angles Ω. Assuming the surface integral on a sphere with the radius R, P_t is expressed by the following equations as in the case of received power.

$$
\begin{aligned}
P_t &= \int_\Omega \Re(S) \cdot \hat{r}d\Omega \\
&= \Re\left\{\int_0^{2\pi}\int_0^\pi (S \cdot \hat{r})R^2 \sin\theta d\theta d\phi\right\} \\
&= w^H C w, \tag{21}
\end{aligned}
$$

$$D = \frac{1}{2}\int_0^{2\pi}\int_0^\pi (\hat{r}_x D_x + \hat{r}_y D_y + \hat{r}_z D_z)R^2 \sin\theta d\theta d\phi, \tag{22}$$

where $C = (D^H + D)/2$ and $\hat{r}$ is a unit vector of r direction in the spherical coordinate. Note that the radius R is set large enough so that only the radiative electromagnetic field becomes dominant. D_x, D_y, and D_z denote the matrices for Poynting vector on the sphere obtained in (12)–(14). From (20) and (21), the BCE is defined as follows:
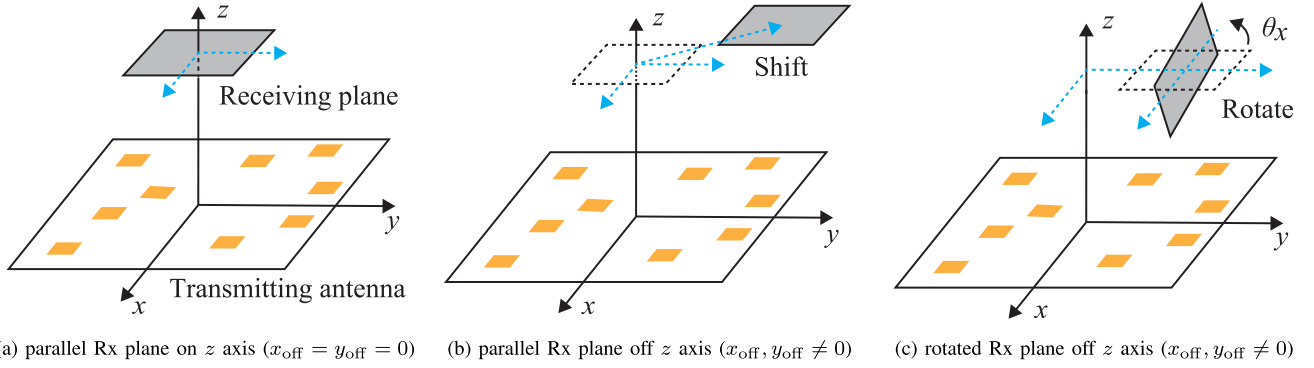
$$BCE = \frac{P_r}{P_t} = \frac{w^H B w}{w^H C w}. \tag{23}$$

The BCE maximization problem is given by the following equation:

$$\max_w BCE = \max_w \frac{w^H B w}{w^H C w}. \tag{24}$$

In this work, matrix B is considered as a positive definite and Hermitian matrix, since the propagation direction of the radiated wave is similar to the direction of the Poynting vector. The matrix C is also considered as a positive definite and Hermitian matrix. In the case, the BCE maximization problem boils down to the generalized eigenvalue problem and (24) is rewritten as follows [5]:

$$Bw_{\text{opt}} = \lambda_{\max}Cw_{\text{opt}}. \tag{25}$$

(a) parallel Rx plane on z axis ($x_{off} = y_{off} = 0$)   (b) parallel Rx plane off z axis ($x_{off}, y_{off} \neq 0$)   (c) rotated Rx plane off z axis ($x_{off}, y_{off} \neq 0$)

FIGURE 2. Calculation models for numerical analysis.

λ_{max} is the maximum eigenvalue and is equal to the maximum BCE, and the optimum array weight $\boldsymbol{w}_{opt}$ giving the maximum BCE is the eigenvector corresponding to λ_{max}. Therefore, the maximum BCE and the optimum array weight can be obtained by solving the eigenvalue problem (25).

Although the normal Poynting vector on the Rx plane is utilized for the calculation of the received power, the described method can also calculate the received power including the polarization direction of the Rx antenna. Assuming that the complex unit vector of the polarization direction of the Rx antenna is $\hat{\boldsymbol{l}_0}$, the polarization direction of the rotated Rx antenna is given by:

$$\hat{\boldsymbol{l}} = R_z(\theta_z)R_y(\theta_y)R_x(\theta_x)\hat{\boldsymbol{l}_0}. \qquad (26)$$

The received power considering the polarization direction is expressed as follows:

$$
\begin{aligned}
P_r &= \frac{1}{2Z_0} \int_s \left| \boldsymbol{E}(\boldsymbol{r}) \cdot \hat{\boldsymbol{l}} \right|^2 ds \\
&= \boldsymbol{w}^H \left\{ \int_s \frac{\boldsymbol{v}_{e_x}\boldsymbol{v}_{e_x}{}^H |\hat{l}_x|^2 + \boldsymbol{v}_{e_y}\boldsymbol{v}_{e_y}{}^H |\hat{l}_y|^2 + \boldsymbol{v}_{e_z}\boldsymbol{v}_{e_z}{}^H |\hat{l}_z|^2}{2Z_0} ds \right\} \boldsymbol{w} \\
&= \boldsymbol{w}^H F \boldsymbol{w}, \qquad (27)
\end{aligned}
$$

$$F = \frac{1}{2Z_0} \int_s \left(\boldsymbol{v}_{e_x}\boldsymbol{v}_{e_x}{}^H |\hat{l}_x|^2 + \boldsymbol{v}_{e_y}\boldsymbol{v}_{e_y}{}^H |\hat{l}_y|^2 + \boldsymbol{v}_{e_z}\boldsymbol{v}_{e_z}{}^H |\hat{l}_z|^2 \right) ds, \qquad (28)$$

where Z_0 denotes the wave impedance in the free space. The BCE maximization problem considering the polarization direction of the Rx antenna is given by using (27) instead of (20) in (24). Since F is considered as a positive definite and Hermitian matrix, the BCE maximization problem considering the polarization direction of the Rx antenna also boils down to the generalized eigenvalue problem. In this work, the maximization problem (25) was solved based on the Poynting vector, unless otherwise stated.

III. NUMERICAL ANALYSIS

In this section, the numerical analysis of the BCE maximization for various calculation models without mutual coupling is described. Fig. 2 presents the calculation models: parallel Rx plane on the z axis, parallel Rx plane off the

TABLE 1. The conditions in the numerical analysis.

condition	Tx antenna	z position of Rx plane
(a)	10×10 array	$z_{off} = 1.5$ m
(b)	20×20 array	$z_{off} = 6$ m

z axis, and rotated Rx plane off the z axis. For comparison, the calculation results using the optimized array weight obtained through the BCE maximization in the far field are also presented in the subsections about the models presented in Fig. 2(a) and Fig. 2(b). For the BCE maximization in the far field, we used the optimization method proposed in [5]. The quadratic phase taper was provided to focus on the center of Rx plane, so that the obtained results in the far field can be applied to the near field. In the numerical analysis, the composite Simpson's rule was applied to calculate the integral of the matrices in (18), (22), and (28) . By using the eig function in MATLAB, the generalized eigenvalue problems were solved. In the numerical analysis, the frequency is 5.8 GHz, and the x and y element spacings are half the wavelength. Table 1 presents the employed simulation condition of the Tx antenna and the z position of Rx plane. When the Tx antennas are the 10×10 and 20×20 arrays, the ranges of the Fresnel region are 0.36 m–2.58 m and 1.01 m–10.3 m, respectively. In this work, circular patch antennas were used as the elements in the array antenna. The theoretical E-field pattern of the circular patch antenna is given as follows [15]:

$$E_\theta = -ja \cos\phi \sin(k_0 t \cos\theta) \frac{J_1'(k_0 a \sin\theta)}{\cos\theta}, \qquad (29)$$

$$E_\phi = j \sin\phi \sin(k_0 t \cos\theta) \frac{J_1(k_0 a \sin\theta)}{k_0 \sin\theta}, \qquad (30)$$

where a and t denote the patch radius and substrate thickness, respectively, and we set $a = 8.74$ mm and $t = 1.53$ mm. J_1 denotes the Bessel function of the first kind. In this work, the polarization direction of the antenna was set to the x direction.

A. PARALLEL RECEIVING PLANE ON THE Z AXIS

The calculation model is presented in Fig. 2(a), where the Rx plane is on the z axis and parallel with the Tx antenna. Fig. 3 presents the calculated BCE when sweeping the length
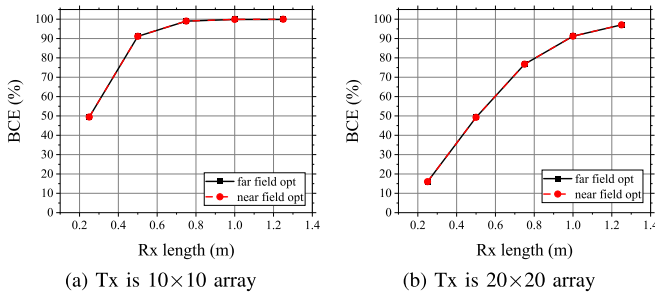
(a) Tx is 10×10 array

(b) Tx is 20×20 array

FIGURE 3. Calculated BCE results when sweeping the length of square Rx plane in the conditions presented in Table 1.
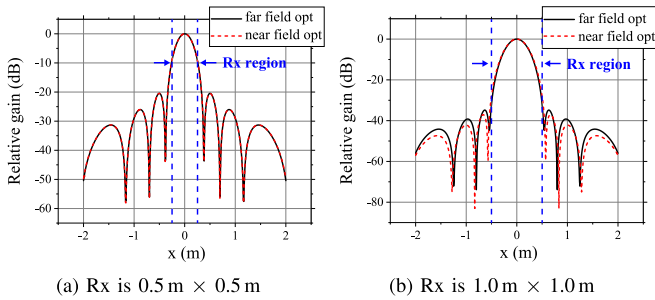

(a) Rx is 0.5 m × 0.5 m

(b) Rx is 1.0 m × 1.0 m

FIGURE 4. Calculated pattern of the *z* component of the Poynting vector on *y* = 0 m and *z* = 1.5 m when the Tx antenna is the 10 × 10 array antenna. (a) The Rx plane is 0.5 m × 0.5 m. (b) The Rx plane is 1.0 m × 1.0 m.

(a) Tx is 10 × 10 array

(b) Tx is 20 × 20 array

FIGURE 5. Calculated BCE results when sweeping the *x*, *y* offset values.

(a) far field opt

(b) near field opt

FIGURE 6. Amplitude distribution of 10 × 10 array when $x_{off} = y_{off} = 1.5$ m.

(a) far field opt

(b) near field opt

FIGURE 7. Phase distribution of 10 × 10 array when $x_{off} = y_{off} = 1.5$ m.

of the square Rx in the conditions presented in Table 1. Note that in the far-field optimization, we set the annular region of the Rx plane as $-u_0 \leq u, v \leq u_0$, where $u = \sin\theta\cos\phi$, $v = \sin\theta\sin\phi$, $u_0 = \sin\theta_0$, $\theta_0 = \arctan(L_{Rx}/2z_{off})$, and L_{Rx} denotes the length of the Rx plane. In both cases, the obtained BCEs were almost the same when near- and far-field optimizations were employed. The results agree with the theory that the near-field radiation pattern on the Rx plane can be approximated to the far-field pattern when using the array weight obtained in the far-field optimization with a quadratic phase taper to focus on the Rx plane. Fig. 4 presents the calculated normal Poynting vector patterns on the Rx plane when the Tx antenna is the 10×10 array. From the figure, it can be seen that the level of the side lobe is lower in the case of the near-field optimization when the Rx plane is larger. This result indicates that the near-field optimization yields a better result for a larger Rx plane as the paraxial approximation does not hold when utilizing the results obtained in the far-field optimization.

B. PARALLEL RECEIVING PLANE OFF THE Z AXIS

In Fig. 2(b), the calculation model is presented, where the Rx plane is off the *z* axis and parallel with the Tx antenna. For conditions (a) and (b) presented in Table 1, the Rx dimensions were set to 0.5 m × 0.5 m and 1.0 m × 1.0 m, respectively. In the two conditions, the center of the Rx was moved to the same distance in the *x* and *y* directions. In Fig. 5, the calculated BCE is presented. Since it is difficult to define the angular region for the Rx plane off the *z* axis, the results of the far-fie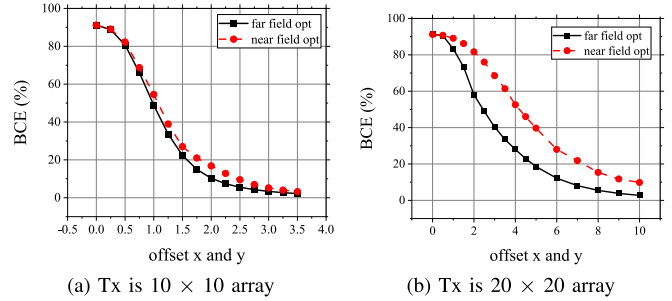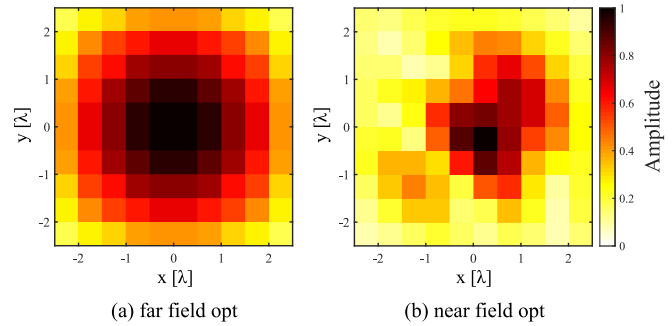ld optimization were obtained by using the optimized array weight when the Rx plane was on the *z* axis and by providing the quadratic phase taper to focus on the center of the Rx plane at each *x*, *y* offset value. In other words, the BCE was calculated by scanning the beam to the center of the Rx plane with a constant amplitude distribution. Based on the results presented in Fig. 5, the BCE obtained through the near-field optimization was higher than that obtained through the far-field optimization. Moreover, it further increased as the array element increased. In the results obtained through the far-field optimization, the beam width became larger with the increase in the *x*, *y* offset value due to the constant amplitude distribution. Conversely, in the results obtained through the near-field optimization, the beam width was narrow due to the optimization of the beam pattern for each *x*, *y* offset point. Fig. 6 and Fig. 7 present the amplitude and phase distribution of the 10 × 10 array when $x_{off} = y_{off} = 1.5$ m, respectively. The parts with a large amplitude were biased in the *x*, *y* offset direction in the near-field optimization. In Fig. 8, the patterns of the
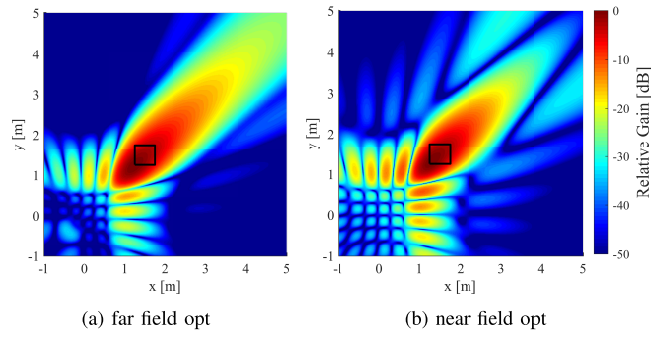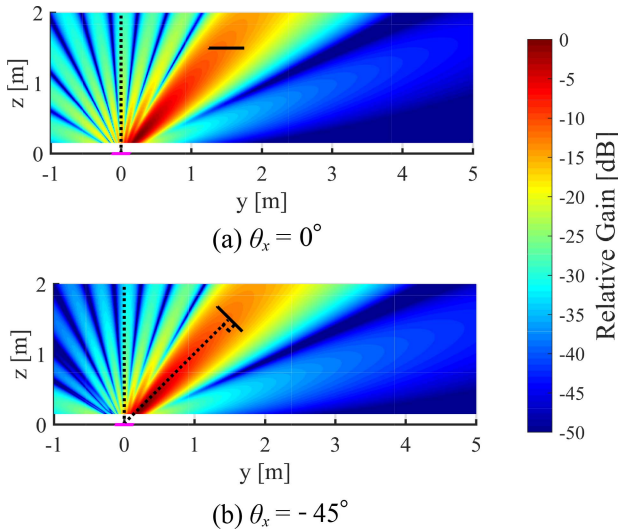
FIGURE 8. Calculated patterns of the *z* component of the Poynting vector on the *xy* plane when the Tx antenna is the 10 × 10 array and $x_{off} = y_{off} = 1.5$ m. The black lines indicate the Rx plane.
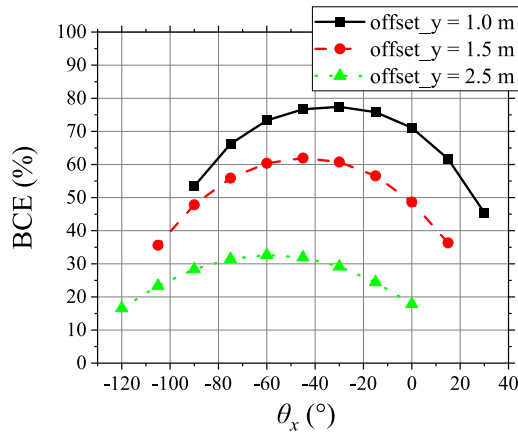

**FIGURE 9.** Calculated BCE results when sweeping the θ_x at each offset point.

FIGURE 10. Calculated patterns of the normal Poynting vector to the Rx plane on the *yz* plane at *x* = 0 m. The black and magenta solid lines indicate the Rx plane and the Tx antenna, respectively.

normal Poynting vector on the Rx plane when using the array weight shown in Fig. 6 and Fig. 7 are presented. The beam width in the result obtained through the near-field optimization was found to be narrow, although the side lobes were larger, which resulted in the improvement of BCE.
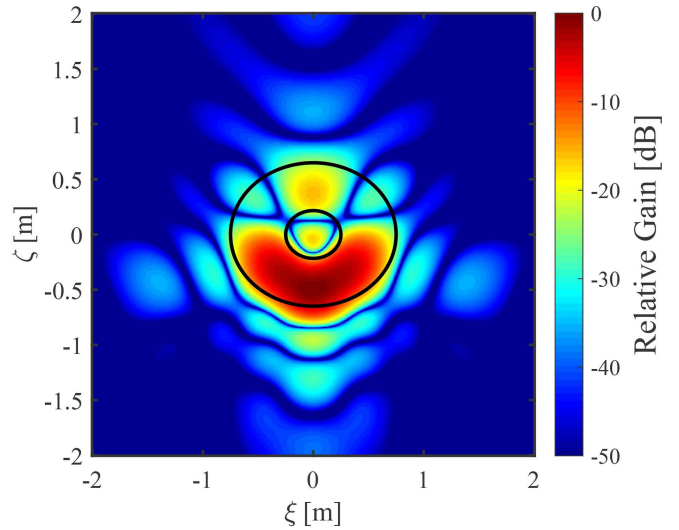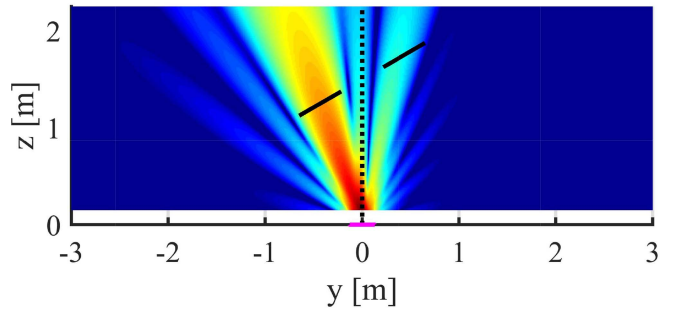
FIGURE 11. Calculated patterns of the normal Poynting vector to the Rx plane. The black and magenta solid lines indicate the Rx plane and the Tx antenna, respectively.

Based on the above results, for the Rx plane off the *z* axis, the near-field optimization yields higher BCE than scanning the beam obtained via the far-field optimization, especially with a large Tx array antenna.

C. ROTATED RECEIVING PLANE OFF THE Z AXIS

In Fig. 2(c), the calculation model is presented, where the Rx plane is off the *z* axis and not parallel with the Tx antenna. In condition (a) presented in Table 1, the dimension of the Rx plane is set to 0.5 m × 0.5 m, $y_{off} = 1.0$ m, 1.5 m, 2.5 m, and $x_{off} = 0$ m. In these conditions, the rotation angle for the *x* axis was changed, and the obtained BCE results are presented in Fig. 9. The BCE was found to have the maximum value at the specific rotation angle, where the vector from the center of Tx antenna to the center of the rotated Rx plane becomes perpendicular to the Rx plane. In Fig. 10, the patterns of the normal Poynting vector to the Rx plane on the *yz* plane when $\theta_x = 0°$, $-45°$, and $y_{off} = 1.5$ m are presented. Note that in this case, $\theta_x = -45°$ gives the maximum BCE. From the figure, it can be seen that the side lobes are small when $\theta_x = -45°$.

Next, to confirm that the proposed method can deal with an arbitrary Rx plane, optimization for a rotated annular-ring

plane was conducted. The inner and outer radii are 0.25 m and 0.75 m, respectively, and the center is located at $x = y = 0$ and $z = 1.5$ m. The rotation angles are $\theta_x = 30°$ and $\theta_y = \theta_z = 0°$. Fig. 11 presents the calculated patterns of the normal Poynting vector to the Rx plane. In Fig. 11(a), ξ and ζ indicate the rotated x and y axes, respectively. The radiated power was concentrated within the annular ring, especially in the part near the transmitting antenna. The BCE was 98.03 %. These results confirm that the proposed method is available for an arbitrary Rx plane.

IV. OPTIMIZATION WITH MUTUAL COUPLING
A. OPTIMIZATION IN A LINEARLY POLARIZED ARRAY
Since the proposed method deals with each element pattern, the BCE optimization including mutual coupling can be applied. For the inclusion of mutual coupling, the active element patterns obtained in the electromagnetic (EM) simulation were used. An active element pattern is defined as a pattern created when feeding a single element in the array and terminating all the other array elements in the matched loads [16]. The active element patterns are related to the active reflection coefficients, which are expressed by an equation including the active reflection coefficients. Thus, an active element pattern includes the fluctuation of radiation pattern by mutual coupling and edge effect in the array [16], [17]. In this work, the matched loads are set to 50 Ω, and CST Studio Suite was used for the EM simulation. In Fig. 12, the simulation model of a linearly polarized single circular patch antenna and the 5×5 array are presented. The design frequency is 5.8 GHz, and the used substrate parameter is as follows: the substrate thickness is 1.58 mm, the dielectric constant is 2.6, the dielectric loss tangent is 0.0018, and the copper thickness is 18 μm. In the 5×5 array model, the element spacing is 0.5λ, and the array dimension is 2.5λ × 2.5λ. For the 5×5 array, the range of the Fresnel region is 0.13 m-0.65 m. Fig. 13 presents the simulation flows with or without consideration of the influence of mutual coupling on the BCE optimization. To obtain the optimized array weight, we firstly solved the BCE maximization problem in the numerical analysis by using the element patterns obtained from the EM simulation in each model. Note that when the obtained pattern from the single element model is used, the optimization results do not reflect the influence of mutual coupling. Conversely, when the obtained active element patterns from the 5×5 array are used, the optimization results reflect the influence of mutual coupling. Then, we conducted the EM simulation in the 5×5 array model by using the array weight obtained through the BCE optimization.

At first, the used simulation condition is as follows: the parallel Rx plane is on the z axis ($z = 0.4$ m), and the dimension is 0.25 m × 0.25 m. The results of the EM simulation are presented in Table 2, and the quantities are defined as follows: The transmission efficiency η is defined as the ratio of the received power on the Rx plane and the total input power to the array. The reflection loss Γ is defined as the ratio of the total reflected power at all input ports and the total input
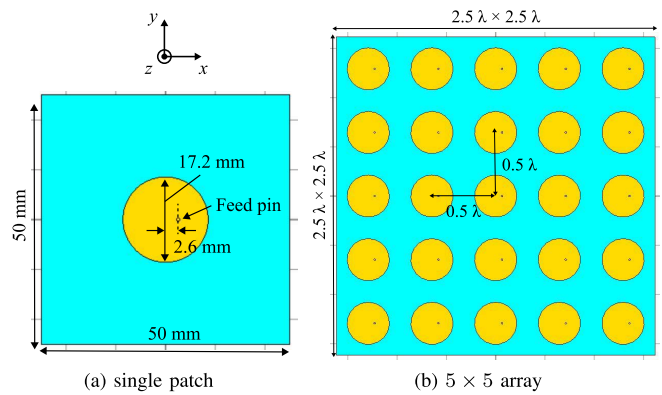

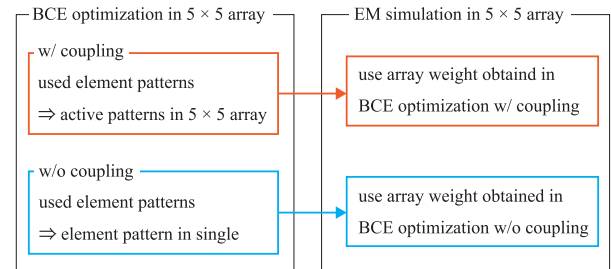**FIGURE 12.** Simulation models of the linearly polarized array antenna in CST.

FIGURE 13. Simulation flows with or without inclusion of mutual coupling in the BCE optimization.

TABLE 2. EM simulation results when the Tx antenna is the 5 × 5 array, the parallel Rx dimension is 0.25 m × 0.25 m, $x_{off} = y_{off} = 0$ m, and $z_{off} = 0.4$ m.

w/ or w/o coupling in BCE optimization	w/o coupling	w/ coupling
Transmission efficiency [%]	76.20	77.09
BCE [%]	86.45	87.02
Reflection loss [%]	8.89	8.44
Radiation efficiency [%]	96.75	96.75

TABLE 3. EM simulation results when the Tx antenna is the 5 × 5 array, the parallel Rx dimension is 0.25 m × 0.25 m, $x_{off} = y_{off} = 0.3$ m, and $z_{off} = 0.4$ m.

w/ or w/o coupling in BCE optimization	w/o coupling	w/ coupling
Transmission efficiency [%]	25.99	38.15
BCE [%]	38.61	42.51
Reflection loss [%]	24.59	5.53
Radiation efficiency [%]	89.27	95.00

power to the array. The radiation efficiency η_{rad} is defined as the ratio of the total radiated power and the total accepted power at all input ports. These quantities and BCE have the following relationship: $\eta = (1 - \Gamma)\eta_{rad}BCE$. By considering mutual coupling in the BCE optimization, BCE increased and the reflection loss decreased by 0.57 and 0.45 points, respectively. As a result, the transmission efficiency increased by 0.89 points compared with the case without consideration of mutual coupling.

Next, we set the simulation condition where the Rx plane is moved 0.3 m in the x and y directions. The other parameters are the same as those mentioned above. The results of the EM simulation are presented in Table 3. By considering mutual

(a) single patch (b) 5 × 5 array
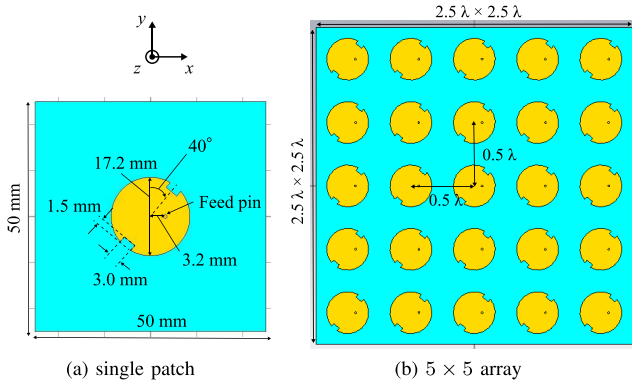
FIGURE 14. Simulation models of circularly polarized array antenna in CST.

(a) w/o coupling (b) w/ coupling
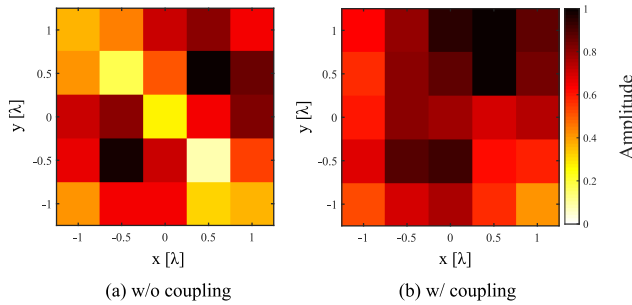
FIGURE 15. Obtained amplitude distribution through BCE optimization.

(a) w/o coupling (b) w/ coupling
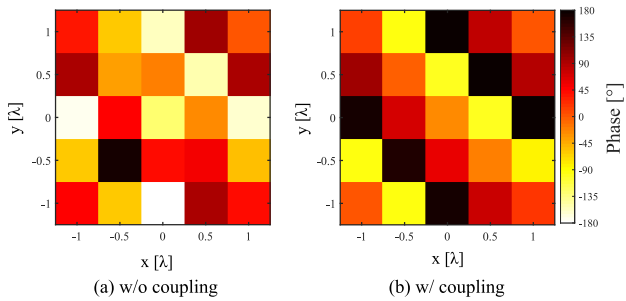
FIGURE 16. Obtained phase distribution through BCE optimization.

TABLE 4. EM simulation results when the Tx antenna is the circularly polarized 5 × 5 array; the parallel Rx dimension is 0.25 m × 0.25 m, $x_{off} = y_{off} = 0.3$ m, and $z_{off} = 0.4$ m.

w/ or w/o coupling in BCE optimization	w/o coupling	w/ coupling
Transmission efficiency [%]	24.58	39.29
BCE [%]	34.74	43.45
Reflection loss [%]	18.64	5.40
Radiation efficiency [%]	86.98	95.59

coupling in the BCE optimization, the BCE and radiation efficiency increased by 3.90 and 5.73 points, respectively. In addition, the reflection loss decreased by 19.06 points compared with the case without consideration of mutual coupling. This is attributed to the relation between the active element patterns and the active reflection coefficients; the influence of active reflection coefficients is reflected in the fluctuation of element pattern and the gain reduction. As a result, the transmission efficiency improved by 12.16 points.

(a) w/o coupling (b) w/ coupling
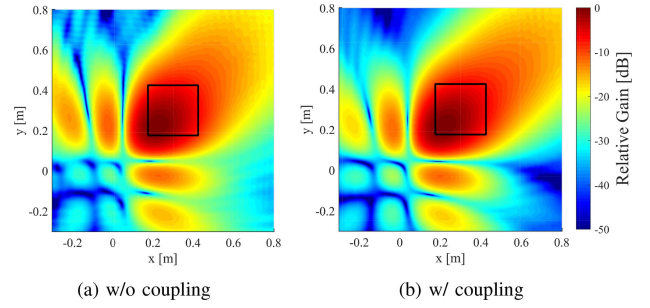
FIGURE 17. EM simulation results of the LHCP pattern on the *xy* plane at *z* = 0.4 m. The black lines indicate the Rx plane.

(a) w/o coupling (b) w/ coupling
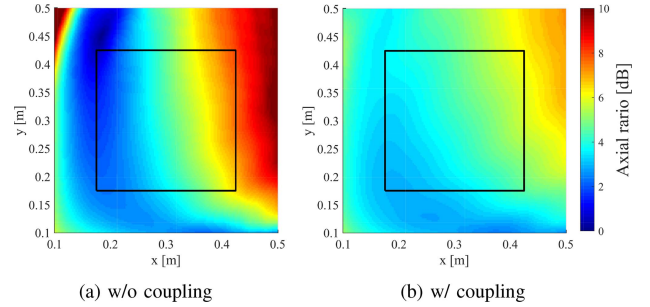
FIGURE 18. EM simulation results of the axial ratio on the *xy* plane at *z* = 0.4 m. The black lines indicate the Rx plane.

In general, the influence of mutual coupling is larger when scanning the beam. This is the reason why the improvement was larger than when the Rx plane was on the *z* axis. Based on these results, it can be confirmed that the proposed method using active element patterns is useful and provides better results, especially when scanning the beam.

B. OPTIMIZATION IN A CIRCULARLY POLARIZED ARRAY

To investigate the validity of the optimization method with consideration of the polarization direction of Rx antenna, a simulation in the left-hand circularly polarized array model presented in Fig. 14 was conducted in the similar manner to the linearly polarized array. To consider the component of the left-hand circular polarization (LHCP) in the BCE optimization, we used (27) instead of (20) and solved the maximization problem (25). The design frequency is 5.8 GHz, and the element spacing is 0.5 λ. Moreover, the substrate parameters are the same as those mentioned in the previous subsection. The used simulation condition is as follows: the parallel Rx dimension is 0.25 m × 0.25 m and $x_{off} = y_{off} = 0.3$ m, and $z_{off} = 0.4$ m. In Table 4, the simulation results are presented. By considering mutual coupling in the BCE optimization, the transmission efficiency was significantly improved by 14.71 points, as described in the case of linear polarized array. Fig. 15 and Fig. 16 present the obtained amplitude and phase distribution obtained through the BCE optimization. From these figures, it can be seen that the optimum array weights differ greatly depending on whether or not mutual coupling is considered. Fig. 17 and Fig. 18 present the results of the LHCP pattern and axial ratio on the *xy* plane at *z* = 0.4 m, respectively. The side lobe

and the axial ratio were found to be small by considering the influence of mutual coupling. The above results support the validity of the method considering the polarization direction of Rx antenna.

V. CONCLUSION

In this work, the array optimization method for maximum BCE to an arbitrary Rx plane in the near field has been introduced. Optimization with mutual coupling by using active element patterns can be performed in this method. Since the problem of BCE maximization boils down to the generalized eigenvalue problem, the best solution can be obtained mathematically. This method has been confirmed to yield better results than the application of the optimum far-field pattern into the near field, particularly when the Rx plane is large and off the z axis. Besides, the numerical results have proved that the proposed method can maximize the BCE for an arbitrary Rx plane. From the results of the EM simulation, we have found that the BCE optimization using the active element patterns decreases the antenna and reflection losses and increases the BCE. This is the reason for the improvement of the transmission efficiency, especially when the Rx plane is off the z axis. Moreover, the results in LHCP antenna model have shown that the proposed method can maximize BCE with consideration of the polarization direction of the receiving antenna. If the array antenna is sufficiently large to ignore the edge effect, the individual active element patterns are approximately identical [17]. In this case, the active element patterns obtained in the infinite array model can be utilized as active element patterns in the large finite array. The proposed method is also applicable for an arbitrary planar array, although the Tx antennas used in this work were the square arrays.

REFERENCES

[1] W. C. Brown, "The history of power transmission by radio waves," *IEEE Trans. Microw. Theory Techn.*, vol. 32, no. 9, pp. 1230–1242, Sep. 1984.
[2] N. Shinohara, "Power without wires," *IEEE Microw. Mag.*, vol. 12, no. 7, pp. S64–S73, Dec. 2011.
[3] N. Shinohara, Ed., *Recent Wireless Power Transfer Technologies via Radio Waves*. Gistrup, Denmark: River Publ., 2018.
[4] S. Prasad, "On an index for array optimization and the discrete prolate spheroidal functions," *IEEE Trans. Antennas Propag.*, vol. 30, no. 5, pp. 1021–1023, Sep. 1982.
[5] G. Oliveri, L. Poli, and A. Massa, "Maximum efficiency beam synthesis of radiating planar arrays for wireless power transmission," *IEEE Trans. Antennas Propag.*, vol. 61, no. 5, pp. 2490–2499, May 2013.
[6] A. F. Morabito, A. R. Laganà, and T. Isernia, "Optimizing power transmission in given target areas in the presence of protection requirements," *IEEE Antennas Wireless Propag. Lett.*, vol. 14, pp. 44–47, Sep. 2015.
[7] A. F. Morabito, "Synthesis of maximum-efficiency beam arrays via convex programming and compressive sensing," *IEEE Antennas Wireless Propag. Lett.*, vol. 16, pp. 2404–2407, Jun. 2017.
[8] X. Li, B. Duan, and L. Song, "Design of clustered planar arrays for microwave wireless power transmission," *IEEE Trans. Antennas Propag.*, vol. 67, no. 1, pp. 606–611, Jan. 2019.
[9] X. Li, B. Duan, J. Zhou, L. Song, and Y. Zhang, "Planar array synthesis for optimal microwave power transmission with multiple constraints," *IEEE Antennas Wireless Propag. Lett.*, vol. 16, pp. 70–73, Apr. 2016.
[10] X. Li, K. M. Luk, and B. Duan, "Aperture illumination designs for microwave wireless power transmission with constraints on edge tapers using bezier curves," *IEEE Trans. Antennas Propag.*, vol. 67, no. 2, pp. 1380–1385, Feb. 2019.
[11] X. Li, K. Luk, and B. Duan, "Multiobjective optimal antenna synthesis for microwave wireless power transmission," *IEEE Trans. Antennas Propag.*, vol. 67, no. 4, pp. 2739–2744, Apr. 2019.
[12] J. W. Sherman, "Properties of focused apertures in the Fresnel region," *IRE Trans. Antennas Propag.*, vol. 10, no. 4, pp. 399–408, Jul. 1962.
[13] X. Cai and W. Geyi, "An optimization method for the synthesis of flat-top radiation patterns in the near- and far-field regions," *IEEE Trans. Antennas Propag.*, vol. 67, no. 2, pp. 980–987, Feb. 2019.
[14] V. N. Garmash and S. S. Shaposhnikov, "Matrix method synthesis of transmitting antenna for wireless power transmission," *IEEE Trans. Aerosp. Electron. Syst.*, vol. 36, no. 4, pp. 1142–1148, Oct. 2000.
[15] S. A. Long, L. C. Shen, and P. B. Morel, "Theory of the circular-disc printed-circuit antenna," *Proc. Inst. Elect. Eng.*, vol. 125, no. 10, pp. 925–928, Oct. 1978.
[16] D. M. Pozar, "The active element pattern," *IEEE Trans. Antennas Propag.*, vol. 42, no. 8, pp. 1176–1178, Aug. 1994.
[17] D. M. Pozar, "A relation between the active input impedance and the active element pattern of a phased array," *IEEE Trans. Antennas Propag.*, vol. 51, no. 9, pp. 2486–2489, Sep. 2003.

SEISHIRO KOJIMA (Graduate Student Member, IEEE) received B.E. degree in electrical and electronic engineering and the M.E. degree in electric engineering from the University of Kyoto in 2015 and 2017, respectively, where he is currently pursuing the Ph.D. degree in electric engineering. His current research interests include antenna design, microwave circuits and beamforming technique for microwave power transmission. He is a student member of the Institute of Electronics, Information and Communication Engineers.

TOMOHIKO MITANI (Member, IEEE) received the B.E. degree in electrical and electronic engineering, the M.E. degree in informatics, and the Ph.D. degree in electrical engineering from Kyoto University, Kyoto, Japan, in 1999, 2001, and 2006, respectively, where he was an Assistant Professor with the Radio Science Center for Space and Atmosphere in 2003. Since 2012, he has been an Associate Professor with the Research Institute for Sustainable Humanosphere, Kyoto University. His current research interests include microwave heating systems, magentrons, and wireless power transfer systems via microwaves. He has been the treasurer of IEEE MTT-S Kansai Chapter since 2014. He is a member of the Institute of Electronics, Information and Communication Engineers and the Japan Society of Electromagnetic Wave Energy Applications (JEMEA). He has been a Board Member of JEMEA since 2015.

NAOKI SHINOHARA (Senior Member, IEEE) received the B.E. degree in electronic engineering, the M.E. and Ph.D. (Eng.) degrees in electrical engineering from Kyoto University, Japan, in 1991, 1993, and 1996, respectively. He was a Research Associate with Kyoto University in 1996, where he has been a Professor since 2010. He has been engaged in research on solar power station/satellite and microwave power transmission systems. He was a Lecturer of IEEE MTT-S Distinguish Microwave from 2016 to 2018. His books include *Wireless Power Transfer via Radiowaves* (ISTE Ltd. and Wiley), *Recent Wireless Power Transfer Technologies via Radio Waves* (ed., River Publishers), and *Wireless Power Transfer: Theory, Technology, and Applications* (ed., IET), and some Japanese text books on WPT. He is a Former Chair of the IEEE MTT-S Technical Committee 25 (Wireless Power Transfer and Conversion), a TPC Member of the IEEE MTT-S Kansai Chapter, a Founder and an Advisory Committee Member of the IEEE Wireless Power Transfer Conference, a Vice Chair of URSI Commission D, an Executive Editor of *International Journal of Wireless Power Transfer* (Cambridge Press), the First Chair and a Technical Committee Member on IEICE Wireless Power Transfer, an adviser to the Japan Society on Electromagnetic Wave Energy Applications, the Vice Chair of the Space Solar Power Systems Society, and the Chair of the Wireless Power Transfer Consortium for Practical Applications (WiPoT) and the Wireless Power Management Consortium.